Journal of Catalysis 260 (2008) 128–133

Contents lists available at ScienceDirect

Journal of Catalysis

www.elsevier.com/locate/jcat

Synthesis of visible-light-active TiO_2-based photocatalysts by carbon and nitrogen doping

Xiangxin Yang [a], Chundi Cao [a], Larry Erickson [a], Keith Hohn [a], Ronaldo Maghirang [b], Kenneth Klabunde [c,*]

[a] Department of Chemical Engineering, Kansas State University, Manhattan, KS 66506, USA
[b] Department of Biological and Agricultural Engineering, Kansas State University, Manhattan, KS 66506, USA
[c] Department of Chemistry, Kansas State University, Manhattan, KS 66506, USA

ARTICLE INFO

Article history:
Received 21 April 2008
Revised 27 June 2008
Accepted 12 September 2008
Available online 16 October 2008

Keywords:
Carbon
Nitrogen
TiO_2
Photocatalyst
Visible light
UV

ABSTRACT

TiO_2 has been considered the most promising photocatalyst for the degradation of pollutants in air or water; however, it shows poor absorption of visible light and requires ultraviolet (UV) light for activation. We have successfully synthesized a visible-light-active carbon and nitrogen co-doped TiO_2 catalyst. The catalysts were characterized by X-ray diffraction (XRD), X-ray photoelectron spectroscopy (XPS), Raman spectroscopy, diffuse reflectance spectroscopy (DRS), photoluminescence (PL), and N_2 desorption–adsorption. Our results demonstrate that the optical response of TiO_2 was shifted from UV to the visible light region with the introduction of carbon and nitrogen. Nitrogen was substituted for some of the lattice oxygen atoms, and most of the carbon was in the form of elemental carbon. The surface area of the co-doped catalyst was increased, and its photocatalytic efficiency was enhanced. The photocatalytic tests indicated that the co-doped catalyst demonstrated higher activity for the degradation of methylene blue (MB) compared with pure TiO_2 both under visible light and UV irradiation, attributed to the synergetic effects of carbon and nitrogen dopants.

1. Introduction

Titanium dioxide (TiO_2) has been widely used as a photocatalyst for solar energy conversion and environmental applications (water and air purification) because of good photoactivity, high chemical stability, low cost, and nontoxicity. When TiO_2 is irradiated by light with wavelength (λ) < 387 nm, electrons are promoted across the band gap (3.2 or 3.0 eV in the anatase or rutile crystalline phase, respectively) into the conduction band, leaving holes in the valence band [1–3]. These holes have high oxidation power, then react with adsorbed hydroxide ions to produce hydroxyl radicals, the main oxidizing species responsible for the photooxidation of organic compounds [2]. However, the application of pure TiO_2 is limited, because it requires UV activation. With pure TiO_2, only $<5\%$ of the solar radiation reaching the earth's surface can be used; consequently, considerable effort has been directed toward expanding the optical response of TiO_2 from the UV to the visible light region. One method for doing so is to introduce allowed energy states in the band gap of TiO_2 by doping with transition metal ions such V, W, or Fe [4–7]. But these doped materials are thermally unstable, and these transition metal ions also can act as electron–hole recombination sites, resulting in low photocatalytic efficiency [8,9]. Furthermore, the preparation method, such as the metal-ion implantation method, requires expensive ion implantation facilities, although a large shift in the absorption band toward the visible light region can be obtained [10]. Another approach is to modify TiO_2 with nonmetal atoms, such as S, C, or N. Sulfur-doped TiO_2 has shown high activity for degradation of methylene blue in water under irradiation at wavelengths longer than 440 nm [11]. Lettmann et al. [12] reported the synthesis of coke-containing TiO_2 and its photocatalytic activity under visible irradiation. Ohno et al. [13] found that the absorption edge of TiO_2 was largely shifted from 400 to 700 nm by doping carbonate species into the TiO_2 lattice. Wang et al. [14] prepared a C-doped TiO_2 catalyst using a nonhydrolytic sol–gel method and found that substitutional and interstitial carbon atoms coexisted in the lattice of TiO_2. N-doped TiO_2 has been prepared by direct thermal nitridation of TiO_2 [15,16], amination of TiO_2 [17], sputtering [18,19], and hydrolyzing a titanium precursor in NH_3 [20]. Nakamura et al. [21] proposed that the visible-light response for N-doped TiO_2 arose from an N-induced mid-gap (N 2p) level, formed slightly above the top of the (O 2p) valence band. Asahi et al. [22] theoretically calculated the band structure of the N-doped TiO_2 and concluded that the visible light sensitivity was due to the narrowing of the band gap by mixing the N 2p and O 2p states.

Compared with one nonmetal dopant, doping two kinds of nonmetal atoms has shown more beneficial effects. Li et al. [23] reported that N and F co-doped TiO_2 had higher visible light ac-

* Corresponding author. Fax: +1 785 532 6666.
E-mail addresses: tonyjone568@yahoo.com (X. Yang), kenjk@ksu.edu (K. Klabunde).

0021-9517/$ – see front matter
doi:10.1016/j.jcat.2008.09.016

tivity than N-doped or F-doped TiO_2, because the doped N atoms improved the visible light absorption and the doped F atoms enhanced the surface acidity and the adsorption of agents. The synergetic effects of doped N, S atoms [24] and C, N atoms [25] on the optical shift, crystallinity, surface areas, and activity of TiO_2 also have been studied. We previously reported [26] that C-doped TiO_2 catalyst had high activity for the degradation of acetaldehyde under visible light irradiation. Experimental results suggested that the doped carbon species existed in the form of elemental carbon and was incorporated into the bulk phase of TiO_2. In the present work, we synthesized C and N co-doped TiO_2 photocatalysts by the sol–gel method and tested their photocatalytic activities by degrading methylene blue (MB), which is known to be difficult to degrade under irradiation and often is used as a model dye contaminant to evaluate the activity of a photocatalyst [27–29].

2. Experimental

2.1. Catalyst synthesis

First, 30 mL of deionized water was put into a water-ice bath. Under vigorous stirring, 8 ml of titanium isopropoxide (97%, Aldrich) was added dropwise. The mixture was stirred for 12 h and aged for 24 h. Water removal was accomplished by drying at 80 °C in air. The sample thus obtained was thoroughly ground with an agate mortar pestle and calcined under NH_3 flow at 500 °C for 2 h, then treated in air at 200 °C for 1 h. The sample was designated CN–TiO_2. Pure TiO_2 was prepared by treating the sample in air at 500 °C for 2 h.

2.2. Catalyst characterization

N_2 adsorption–desorption isotherms were obtained at −196 °C on a Nova 1000 series instrument (Quantachrome). The specific surface areas were calculated according to the multipoint BET method. The pore size distributions were calculated from the desorption curve. The BJH method was used to determine the pore volume and pore size. Before adsorption, samples were degassed at 150 °C for 1 h under vacuum.

Raman spectra were recorded using a Nicolet Nexus 670 Fourier transform IR (FTIR) with a Raman module. The system consists of a continuous Nd-YAG (yttrium aluminum garnet) laser (1064 nm) and a liquid nitrogen cooled germanium or InGaAs detector in the 4000–100 cm^{-1} range. The laser power used was in the range of 0.2–0.6 W, with a data point spacing of 3.5 cm^{-1}. The sample was placed in a glass cylindrical Raman cuvette (Nicolet). A typical spectrum contained 128 scans.

X-ray photoelectron spectroscopy (XPS) data were recorded with a Perkin–Elmer PHI 5400 electron spectrometer using acrochromatic Al$K\alpha$ radiation (1486.6 eV). All spectra were obtained under vacuum at a pressure of about 2.0×10^{-9} Torr. The XPS binding energies were measured with a precision of 0.1 eV. The analyzer pass energy was set to 17.9 eV, and the contact time was 50 ms. Before sample testing, the spectrometer was calibrated by setting the binding energies of Au $4f_{7/2}$ and Cu $2p_{3/2}$ to 84.0 and 932.7 eV, respectively. Binding energies for the samples were normalized with respect to the position of the C 1s peak resulting from adsorbed hydrocarbon fragments.

X-ray powder diffraction (XRD) patterns were obtained with a Bruker D8 diffractometer, using Cu$K\alpha$ radiation (1.5406 Å) at 40 kV and 40 mA and a secondary graphite monochromator. Samples were packed into a plastic holder. Measurements were recorded in steps of 0.025°, with a count time of 2 s in the 2θ range of 20°–65°. The phases were identified with the aid of the JCPDS files.

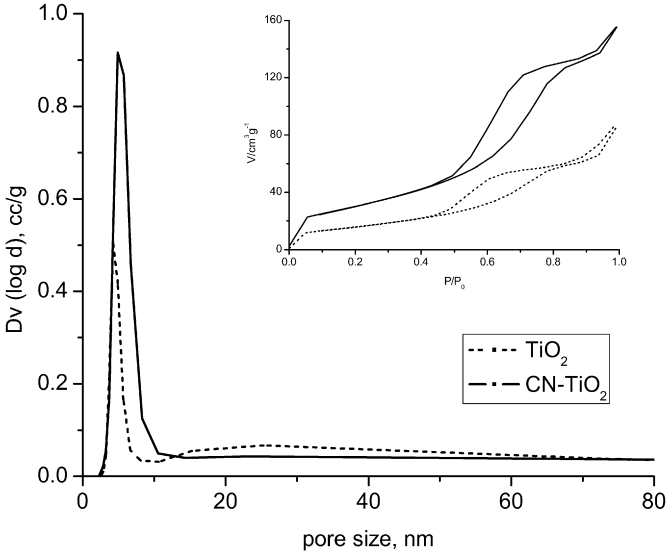

Fig. 1. Pore size distribution and the corresponding isotherm of TiO_2 and CN–TiO_2.

Diffuse reflectance spectra (DRS) were recorded with a Cary 500 Scan UV–vis NIR spectrophotometer with an integrating sphere attachment for diffuse reflectance in the range of 200–800 nm. All spectra were referenced to polytetrafluoroethylene. Photoluminescence (PL) spectra were measured with a fluorospectrophotometer (SPEX Fluoromax-2) using the 280-nm line of a Xe lamp as the excitation source at room temperature.

2.3. Photocatalytic activity measurements

The photocatalytic activities of CN–TiO_2 and TiO_2 catalysts were evaluated by the degradation of MB in an aqueous solution. The light source was am Oriel 1000-W high-pressure Hg arc lamp. The combination of a Vis-NIR long-pass filter (400 nm) and colored glass filter (>420 nm) was used to eliminate UV radiation during visible light experiments. A general procedure was carried out as follows. First, 100 mL of aqueous MB solution (10 mg/L) was placed into a water-jacketed reactor maintained at 25 °C, and then 30 mg of catalyst was suspended in the solution. The suspension was stirred vigorously for 60 min in the dark to establish the adsorption–desorption equilibrium of MB, then irradiated under visible light. Samples were withdrawn from the reactor periodically and centrifuged and analyzed for the degradation of MB using a Cary 500 UV–vis spectrophotometer. MB has a maximum absorbance at 664 nm, which was used as a value for monitoring MB degradation. The absorbance was converted to the MB concentration in accordance with a standard curve showing a linear relationship between the concentration and the absorbance at this wavelength. The same procedure was followed for the UV light experiment by using two cutoff filters ($320 < \lambda < 420$ nm).

3. Results and discussion

3.1. N_2 adsorption–desorption

Fig. 1 shows the pore size distribution curves and nitrogen isotherms of TiO_2 and CN–TiO_2. Both isotherms are type IV with an H2 hysteresis loop, which is characteristic of a mesoporous structure. The textural properties of both samples are summarized in Table 1. The doped TiO_2 had a significantly larger surface area as well as a larger pore size and pore volume and smaller crystallite size, which possibly provided more accessible active sites and enhanced the catalyst activity.

Table 1
Textural properties of TiO_2 and CN–TiO_2.

Sample	S_{BET} (m^2/g)	Pore size (nm)	Pore volume (cm^3/g)
TiO_2	57	4.2	0.14
CN–TiO_2	109	4.9	0.26

3.2. FT-Raman

Raman spectroscopy was successfully applied to probe the phase formation of titanium oxide. It has been reported that six modes—A_{1g} (519 cm^{-1}), B_{1g} (399 and 519 cm^{-1}), and E_g (144, 197, and 639 cm^{-1})—were Raman-active for the anatase phase, whereas four modes—A_{1g} (612 cm^{-1}), B_{1g} (143 cm^{-1}), B_{2g} (826 cm^{-1}), and E_g (447 cm^{-1})—were Raman-active for the rutile phase [30–32]. Fig. 2 shows the Raman spectra of TiO_2 and CN–TiO_2, which suggest that anatase was the predominant phase structure for both samples. By measuring the maximum of low frequency Raman band (peak position and line width), it is possible to determine the crystal dimension, because the particle size can cause large shifts in the location of the scattered Raman peaks and their widths—the quantum size confinement effect [9,33]. Thus, comparing the strongest E_g mode for both samples, the band of CN–TiO_2 was shifted from 145.0 cm^{-1} of TiO_2 to 149.6 cm^{-1}. The full widths at half maximum (FWHM) of this band were 23 cm^{-1} for CN–TiO_2 and 14 cm^{-1} for TiO_2. The increased intensity and broader width of this band indicated that CN–TiO_2 had enhanced crystallinity and smaller particle size, consistent with the results of later XRD measurements. An additional peak at 320 cm^{-1} also appeared in the spectrum of CN–TiO_2, attributed to the first-order scattering of a nonstoichiometric TiN [34].

To gain insight into the change in the Raman spectrum, the spectra in the range of 300–700 cm^{-1} were fitted. In the fitting curves, two other peaks at 460 and 570 cm^{-1} were observed for CN–TiO_2. The peak at 460 cm^{-1} was related to second-order acoustic mode of TiN, and that at 570 cm^{-1} was related to transverse optical mode [35]. Consequently, we concluded that nitrogen was doped and replaced some oxygen atoms in the titanium oxide crystal lattice.

3.3. XPS

XPS measurements were carried out to determine the concentrations of N or C and their chemical states. According to XPS survey spectra of TiO_2 and CN–TiO_2 (not shown here), TiO_2 had only C, O, and Ti elements, whereas CN–TiO_2 had C, O, Ti, and N elements. For TiO_2, the atomic concentrations of the C, O, and Ti elements were 36.2, 48.3, and 15.5 at%, respectively. For CN–TiO_2, the atomic concentrations were 1.8, 42.8, 44.6, and 10.8 at% for the N, C, O, and Ti elements, respectively.

Fig. 3 shows the XPS spectra for CN–TiO_2. The C 1s spectrum showed a single strong peak at 284.6 eV and a weak shoulder at around 288.5 eV. Three forms of carbon species have been detected previously: elemental carbon (285 eV) located within the tetrahedral and octahedral interstices existing within the anatase crystal, a Ti–C bond resulting from substituting oxygen atoms by carbon (281.5 eV), and the carbonate species adsorbed on the surface (288 eV) [36,37]. Therefore, most of the carbon incorporated in the TiO_2 matrix was present as elemental carbon, with only a small amount of carbonate species on the surface. A peak at around 281 eV, reportedly resulting from Ti–C bonds, was not observed in the sample, suggesting that carbon did not substitute for oxygen atom in the lattice of TiO_2.

The N 1s spectra showed 1 peak at 396.2 eV and another at 399.5 eV. An N 1s peak at 400 eV is reportedly related to molecular chemisorbed nitrogen or molecularly adsorbed NO_x or NH_3,

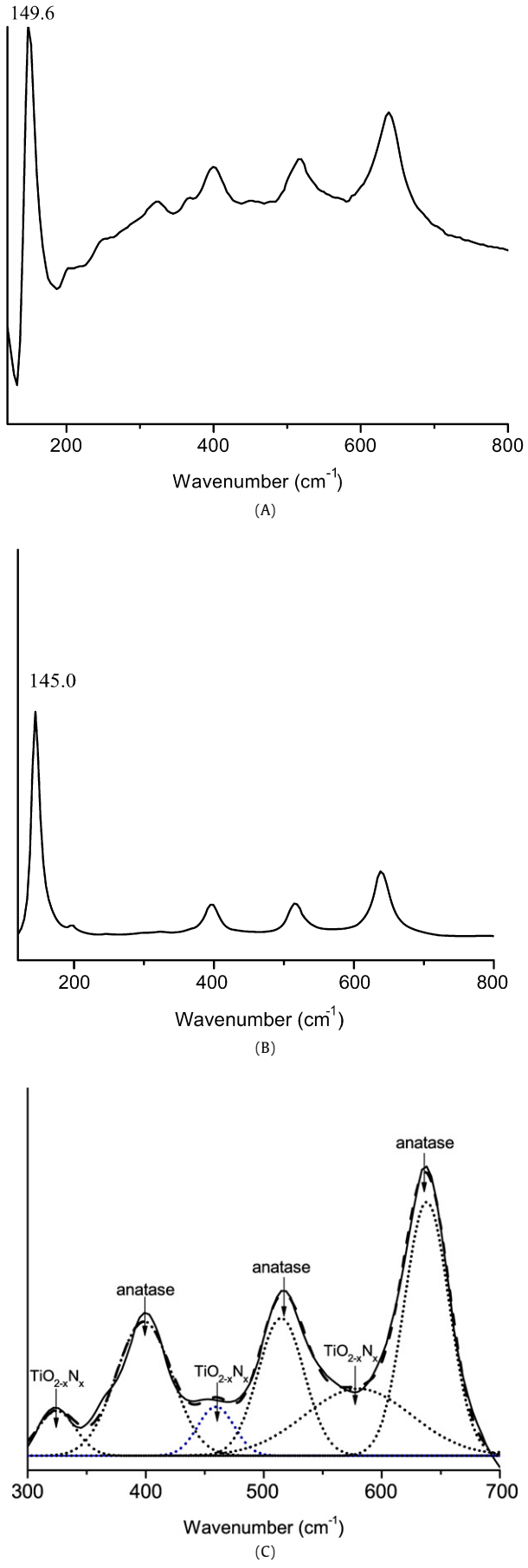

Fig. 2. Raman spectra of CN–TiO_2 (A), TiO_2 (B), and fitting curves for CN–TiO_2 (C).

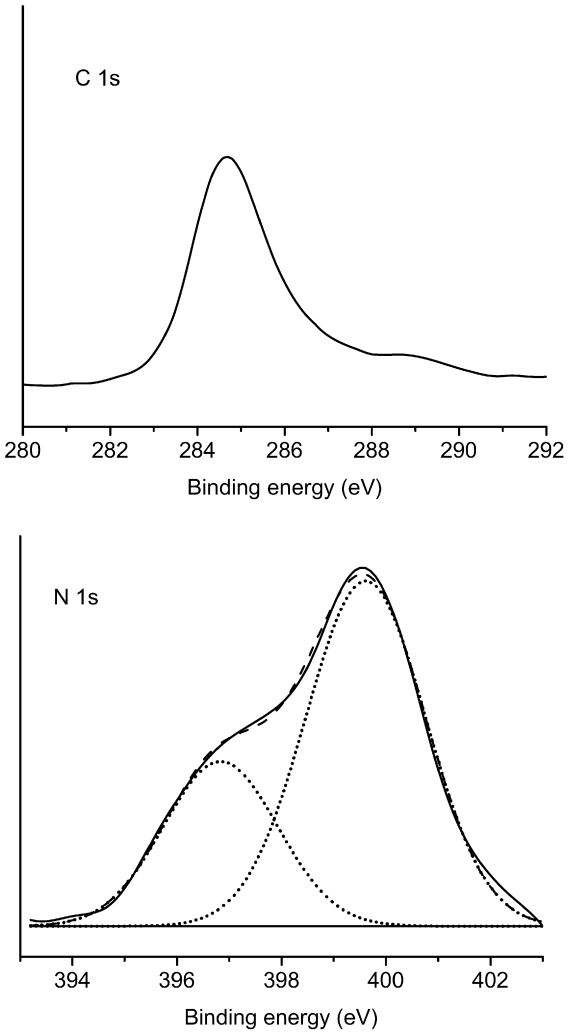

Fig. 3. XPS spectra for C 1s, N 1s of CN–TiO_2.

and a peak at 397.5 eV has been observed in TiN [38–40]. The assignment of the XPS peak of N 1s is somewhat controversial, however. Cong et al. [9] attributed the peak at 399.2 eV to anionic N in O–Ti–N linkages. Prokes et al. [41] found that the N 1s peak for the doped TiO_2-based nanocolloid was broad and centered at 401.3 eV. We attributed the peak at 396 eV to the presence of a Ti–N bond resulting from substitution for oxygen sites by nitrogen atoms in the TiO_2 lattice, which is consistent with previous reports [24,42,43]. These results also coincide with the Raman data displayed in Fig. 2. The feature at 399.5 eV was assigned to adsorbed NH_3 based on our preparation method.

3.4. XRD

Crystal structures of CN–TiO_2 and pure TiO_2 were characterized by XRD. Both samples showed only the anatase phase, with no other crystal phase (rutile or brookite) detected. The strongest peak at $2\theta = 25.3°$, representative of (101) anatase phase reflections, is shown in Fig. 4. Compared with pure TiO_2, the peak position was shifted slightly toward a higher 2θ value, suggesting distortion of the crystal lattice of TiO_2 by the carbon or nitrogen dopants, probably mainly by nitrogen, because nitrogen was substituted for oxygen atoms in the lattice of TiO_2. Fig. 4 also shows that doped TiO_2 had a broader peak than pure TiO_2, indicating the smaller crystallite size of the doped TiO_2. From the FWHM of the diffraction pattern, the crystallite sizes were calculated using Scherrer's equation and were found to be 14 nm for pure TiO_2 and about 9 nm for the doped TiO_2. No diffraction lines due to TiC or TiN were seen, consistent with the XPS results discussed earlier.

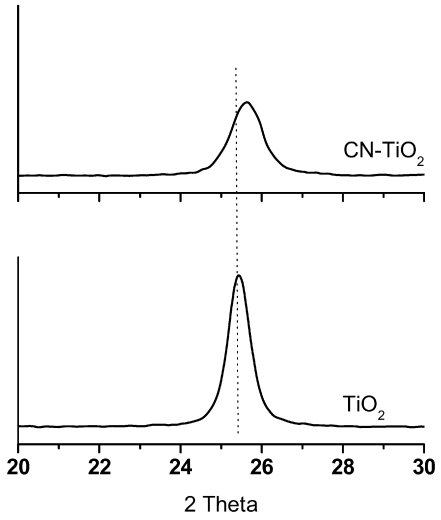

Fig. 4. XRD patterns of CN–TiO_2 and TiO_2.

3.5. DRS

Fig. 5 shows the diffuse reflectance spectra of CN–TiO_2 and TiO_2. As expected, pure TiO_2 exhibited absorption only in the UV region, whereas the optical response of CN–TiO_2 was extended into the visible light region. The visible light absorption for CN–TiO_2 was associated with doped nitrogen and carbon. Carbon can act as a photosensitizer [44], and nitrogen can introduce an impurity level between the valence and conduction band of TiO_2 [21] or narrow the band gap by mixing the N 2p and O 2p states [22]. The band gap energies were calculated according to the equation $E_g = hc/\lambda$, where E_g is the band gap energy (eV), h is the Planck's constant (4.135667×10^{-15} eV s), c is the velocity of light (3×10^8 m/s), and λ is the wavelength (nm) of absorption onset. The band gap energies were 3.05 eV for TiO_2 and 2.12 eV for CN–TiO_2.

3.6. Photoluminescence

PL emission spectra have been widely used to investigate the efficiency of charge carrier trapping, migration, and transfer and to provide insight into the fate of electron–hole pairs in semiconductor particles, because PL emission results from the recombination of free carriers [45,46]. Fig. 6 shows the PL spectra of TiO_2 and CN–TiO_2. The peak at 470–550 nm can be assigned to emission signals originating from the charge-transfer transition of an oxygen vacancy trapped electron [45,46]. The PL intensity of pure TiO_2 was significantly stronger than that of CN–TiO_2. Because the PL emission is the result of the recombination of excited electrons and holes, the lower PL intensity indicates a lower recombination rate of these electrons and holes under light irradiation [45,47,48]. Therefore, the dopants (nitrogen or carbon) quenched the luminescence and enhanced the separation of photoexcited electrons and holes. Because the efficiency of photocatalysis is proportional to the charge carrier (e^- or h^+) transfer rate and inversely proportional to the sum of charge carrier transfer rate and electron–hole recombination rate [2], CN–TiO_2 should have a higher photonic efficiency than the pure TiO_2.

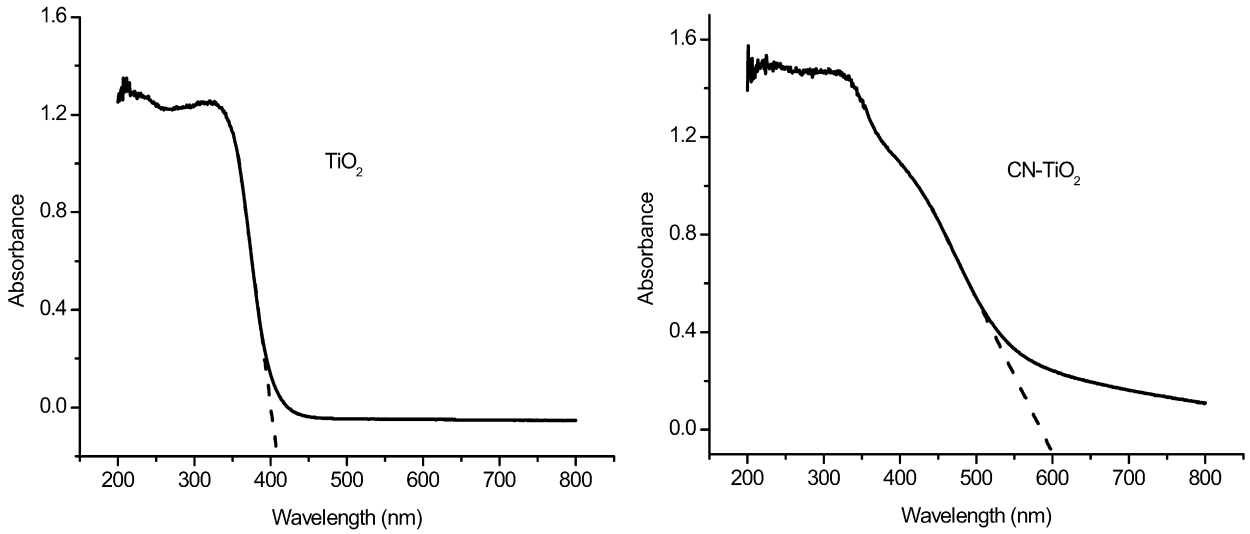

Fig. 5. Diffuse reflectance spectra of TiO_2 and CN–TiO_2.

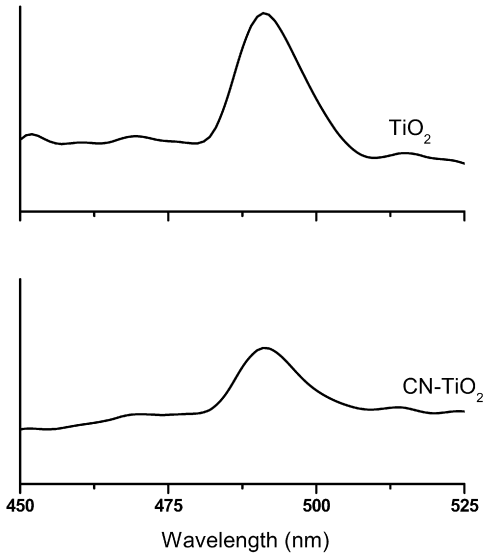

Fig. 6. Photoluminescence emission spectra for TiO_2 and CN–TiO_2 measured at room temperature (excitation wavelength 280 nm).

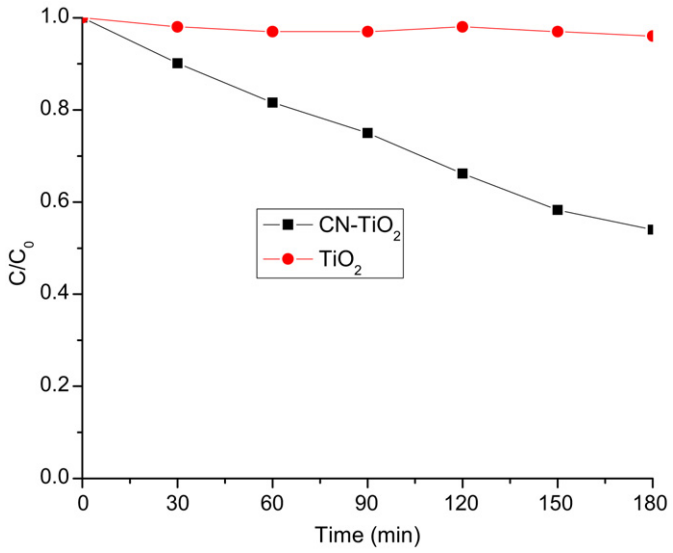

Fig. 7. Degradation of MB on CN–TiO_2 and TiO_2 under visible light irradiation.

3.7. Degradation of MB

3.7.1. Under visible light irradiation

According to diffuse reflectance UV–vis spectra, the optical response of TiO_2 was shifted slightly from UV to the visible light region due to the introduction of carbon and nitrogen. This implied that CN–TiO_2 might be active under visible light irradiation. Fig. 7 depicts the degradation of MB in the presence of CN–TiO_2 and TiO_2 under visible light irradiation. After the desorption–adsorption equilibrium in the dark, the concentration of MB was decreased to 8.5 mg/L for activity testing of CN–TiO_2 and to 9.1 mg/L for TiO_2 testing. To allow better comparisons, we assumed that this was the initial concentration, C_0. It was clear that CN–TiO_2 showed much higher activity in the presence of visible light than pure TiO_2, which exhibited little activity, as expected. If we assumed that the degradation of MB was the first-order reaction (i.e., $dC/dt = -KC$), then the rate constant K for CN–TiO_2 was 0.0035 min^{-1}, 17.5 times greater than that for TiO_2 (0.0002 min^{-1}). This indicates that doping of C and N effectively shifted the optical response from the UV to the visible light region and improved the visible light-induced activity of TiO_2 for the degradation of MB. It was assumed that in our case, the carbon and nitrogen dopants functioned differently for absorption in the visible light region. Carbon acted as a photosensitizer, which could be excited to inject electrons into the conduction band of TiO_2. Subsequently, the electrons could be transferred to surface-adsorbed oxygen molecules and form superoxide anions, which could further transform to $OH^{\bullet}$ and initiate the degradation of MB. For this route to become catalytic, the oxidized carbon might have been reduced by the oxidation of MB or other reactions. In addition, carbon increased the surface area of TiO_2 and improved the adsorption of MB. It is well known that organic compounds should be preconcentrated on the surface of the semiconductor particles to effectively utilize the photoexcitation [49]. For the nitrogen dopant, the substitution for oxygen atoms in the crystal structure of TiO_2 improved the visible light sensitivity by mixing the N 2p and O 2p states or introducing a mid-gap (N 2p) level, formed slightly above the top of the (O 2p) valence band.

3.7.2. Under UV light irradiation

Fig. 8 shows the degradation of MB in the presence of CN–TiO_2 and TiO_2 under UV irradiation. The reaction rate constant, K, was

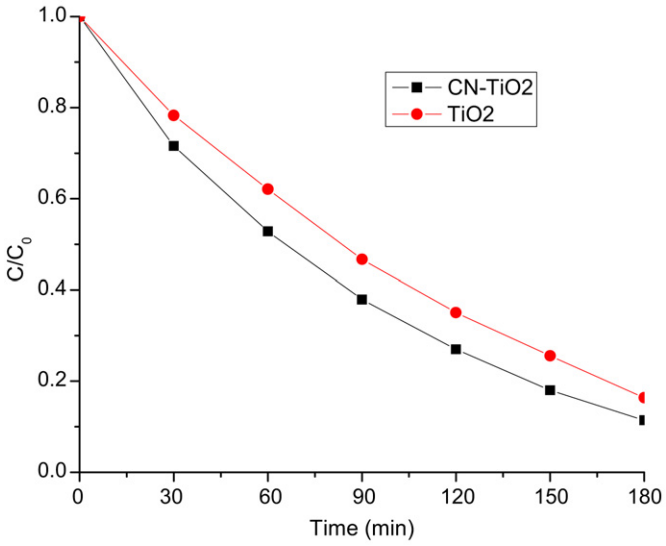

Fig. 8. Degradation of MB on CN–TiO_2 and TiO_2 under UV irradiation.

0.0118 min^{-1} for CN–TiO_2 and 0.0098 min^{-1} for TiO_2. The former value was 20% higher than the latter, possibly due to the increased surface area or enhanced activity. But the PL emission spectra indicate that the carbon and nitrogen dopants enhanced the separation of photoexcited electrons and holes, and thus more electrons and holes should be available in the degradation of MB for CN–TiO_2 under UV irradiation. Therefore, it was highly possible that CN–TiO_2 had higher activity than pure TiO_2 under UV light irradiation.

4. Conclusion

A carbon and nitrogen co-doped TiO_2 (CN–TiO_2) catalyst was successfully synthesized by a simple method. The carbon dopant came from the alkoxide groups of titanium precursor, whereas nitrogen was doped by thermal nitridation. CN–TiO_2 could absorb photoenergy in the visible light region and had a greater surface area than pure TiO_2. The doped elemental carbon acted as a photosensitizer. Nitrogen substituted some oxygen atoms in the lattice of TiO_2, narrowing the band gap by mixing the N 2p and O 2p states or introducing a mid-gap (N 2p) level, which formed slightly above the top of the (O 2p) valence band. Carbon and nitrogen dopants enhanced the separation of photoexcited electrons and holes and improved the photocatalytic efficiency of CN–TiO_2. The co-doped TiO_2 showed higher activity than pure TiO_2 for the degradation of MB under visible light as well as UV irradiation. The high activity was attributed to the several beneficial effects associated with the introduction of carbon and nitrogen.

Acknowledgments

This work was supported by the Army Research Office (through DTRA contract SPO-AA06SP0012), the NanoScale Corporation, and the Kansas State University Targeted Excellence Program.

References

[1] X. Chen, S.S. Mao, Chem. Rev. 107 (2007) 2891.
[2] A.L. Linsebigler, G. Lu, J.T. Yates Jr., Chem. Rev. 93 (1993) 341.
[3] M.A. Fox, M.T. Dulay, Chem. Rev. 95 (1995) 735.
[4] S. Klosek, D. Raftery, J. Phys. Chem. B 105 (2001) 2815.
[5] P.K. Surolia, R.J. Tayade, R.V. Jasra, Ind. Eng. Chem. Res. 46 (2007) 6196.
[6] M.M. Mohamed, M.M. Al-Esaimi, J. Mol. Catal. A 255 (2006) 53.
[7] K.E. Karakitsou, X.E. Verykios, J. Phys. Chem. 97 (1993) 1184.
[8] S. Yang, L. Gao, J. Am. Ceram. Soc. 87 (2004) 1803.
[9] Y. Cong, J. Zhang, F. Chen, M. Anpo, J. Phys. Chem. C 111 (2007) 6976.
[10] M. Anpo, S. Dohshi, M. Kitano, Y. Hu, M. Takeuchi, M. Matsuoke, Annu. Rev. Mater. Res. 35 (2005) 1.
[11] T. Ohno, T. Mitsui, M. Matsumura, Chem. Lett. 32 (2003) 364.
[12] C. Lettmann, K. Hildenbrand, H. Kisch, W. Macyk, W. Maier, Appl. Catal. B 32 (2001) 215.
[13] T. Ohno, T. Tsubota, K. Nishijima, Z. Miyamoto, Chem. Lett. 33 (2004) 750.
[14] X. Wang, S. Meng, X. Zhang, H. Wang, W. Zhong, Q. Du, Chem. Phys. Lett. 444 (2007) 292–296.
[15] H. Chen, A. Nambu, W. Wen, J. Graciani, Z. Zhong, J. Hanson, E. Fujita, J. Rodriguez, J. Phys. Chem. C 111 (2007) 1366.
[16] S. Joung, T. Amemiya, M. Murabayashi, K. Itoh, Chem. Eur. J. 12 (2006) 5526.
[17] C. Burda, Y. Lou, X. Chen, A.C.S. Samia, J. Stout, J.L. Gole, Nano Lett. 3 (2003) 1049.
[18] R. Asahi, T. Morikawa, T. Ohwaki, K. Aoki, Y. Taga, Science 293 (2001) 269.
[19] T. Lindgren, J.M. Mwabora, J. Jonsson, A. Hoel, C.G. Granqvist, S.E. Lindquist, J. Phys. Chem. B 107 (2003) 5709.
[20] T. Ihara, M. Miyoshi, Y. Iriyama, O. Matsumoto, S. Sugihara, Appl. Catal. B 42 (2003) 403.
[21] R. Nakamura, T. Tanaka, Y. Nakato, J. Phys. B 108 (2004) 10617.
[22] R. Asahi, T. Morikawa, T. Ohwaki, K. Aoki, Y. Taga, Science 293 (2001) 269.
[23] D. Li, N. Ohashi, S. Hishita, T. Kolodiazhnyi, H. Haneda, J. Solid State Chem. 178 (2005) 3293.
[24] Y. Xie, Q. Zhao, X. Zhao, Y. Li, Catal. Lett. 118 (2007) 231.
[25] D. Chen, Z. Jiang, J. Geng, Q. Wang, D. Yang, Ind. Eng. Chem. Res. 46 (2007) 2741.
[26] X. Yang, C. Cao, K. Hohn, L. Erickson, R. Maghirang, D. Hamal, K. Klabunde, J. Catal. 252 (2007) 296.
[27] J. Tang, Z. Zou, J. Yin, J. Ye, Chem. Phys. Lett. 382 (2003) 175.
[28] A.A. Belhekar, S.V. Awate, R. Anand, Catal. Commun. 3 (2002) 453.
[29] D. Severino, H.C. Junqueira, M. Gugliotti, D.S. Gabrielli, M.S. Bapista, Photochem. Photobiol. 77 (2003) 459.
[30] H. Berger, H. Tang, F. Kevy, J. Cryst. Growth 130 (1993) 108.
[31] S.P.S. Porto, P.A. Fbeury, T.C. Damen, Phys. Rev. 154 (1967) 522.
[32] S.C. Pillai, P. Periyat, R. George, D.E. McCormack, M.K. Seery, H. Hayden, J. Colreavy, D. Corr, S.J. Hinder, J. Phys. Chem. C 111 (2007) 1605.
[33] D. Bersani, P.P. Lottici, X. Ding, Appl. Phys. Lett. 72 (1998) 73.
[34] E. Gyorgy, A.P.D. Pino, P. Serra, J.L. Morenza, Appl. Surf. Sci. 186 (2002) 130.
[35] Y. Cheng, B.K. Tay, S.P. Lau, H. Kupfer, F. Richter, J. Appl. Phys. 92 (2002) 1845.
[36] X. Wang, S. Meng, X. Zhang, H. Wang, W. Zhong, Q. Du, Chem. Phys. Lett. 444 (2007) 292.
[37] Z. Shi, X. Ye, K. Liang, S. Gu, F. Pan, J. Mater. Sci. 22 (2003) 1255.
[38] H. Irie, Y. Watanabe, K. Hashimoto, J. Phys. Chem. B 107 (2003) 5483.
[39] D. Li, N. Ohashi, S. Hishita, T. Kolodiazhnyi, H. Handea, J. Solid State Chem. 178 (2005) 3293.
[40] N.C. Saha, H.C. Tomkins, J. Appl. Phys. 72 (1992) 3072.
[41] S.M. Prokes, J.L. Gole, X. Chen, C. Burda, W.E. Carlos, Adv. Funct. Mater. 15 (2005) 161.
[42] Q. Li, R. Xie, J. Shang, J. Am. Ceram. Soc. 90 (2007) 1045.
[43] O. Diwald, T.L. Thompson, T. Zubkov, E.G. Goralski, S.D. Walck, J.T. Yates, J. Phys. Chem. B 108 (2004) 6004.
[44] C. Lettmann, K. Hildenbrand, H. Kisch, W. Macyk, W. Maier, Appl. Catal. B 32 (2001) 215.
[45] Y. Cong, J. Zhang, F. Chen, M. Anpo, J. Phys. Chem. C 111 (2007) 6976.
[46] D. Li, H. Haneda, S. Hishita, N. Ohashi, Chem. Mater. 17 (2005) 2596.
[47] H. Tang, K. Prasad, R. Sanjines, P. Schmid, F. Levy, J. Appl. Phys. 75 (1994) 2042.
[48] F.B. Li, X.Z. Li, Chemosphere 48 (2002) 1103.
[49] W. Wang, P. Serp, P. Kalck, J.L. Faria, Appl. Catal. B 56 (2005) 305.